

Quantum Hall effect and semiconductor-to-semimetal transition in biased black phosphorusShengjun Yuan,^{1,*} Edo van Veen,¹ Mikhail I. Katsnelson,¹ and Rafael Roldán^{2,†}¹*Institute for Molecules and Materials, Radboud University, Heijendaalseweg 135, NL-6525 AJ Nijmegen, The Netherlands*²*Instituto de Ciencia de Materiales de Madrid, CSIC, Cantoblanco, E28049 Madrid, Spain*

(Received 8 March 2016; revised manuscript received 11 June 2016; published 28 June 2016)

We study the quantum Hall effect of two-dimensional electron gas in black phosphorus in the presence of perpendicular electric and magnetic fields. In the absence of a bias voltage, the external magnetic field leads to a quantization of the energy spectrum into equidistant Landau levels, with different cyclotron frequencies for the electron and hole bands. The applied voltage reduces the band gap, and eventually a semiconductor-to-semimetal transition takes place. This nontrivial phase is characterized by the emergence of a pair of Dirac points in the spectrum. As a consequence, the Landau levels are not equidistant anymore but follow the $\varepsilon_n \propto \sqrt{nB}$ characteristic of Dirac crystals as graphene. By using the Kubo-Bastin formula in the context of the kernel polynomial method, we compute the Hall conductivity of the system. We obtain a $\sigma_{xy} \propto 2n$ quantization of the Hall conductivity in the gapped phase (standard quantum Hall effect regime) and a $\sigma_{xy} \propto 4(n + 1/2)$ quantization in the semimetallic phase, characteristic of Dirac systems with nontrivial topology.

DOI: 10.1103/PhysRevB.93.245433

I. INTRODUCTION

Black phosphorus (BP) is a direct band gap semiconductor that has been recently exfoliated to obtain atomically thin samples [1–3]. Each BP layer forms a puckered surface due to sp^3 hybridization, revealing a highly anisotropic electrical mobility [4,5], an ambipolar field effect, linear dichroism in optical absorption spectra [2,4,6–8], and anisotropic plasmons [9]. Encapsulation of BP with hexagonal boron nitride has led to high-carrier-mobility devices, with the observation of quantum magneto-oscillations [10–14] and the integer quantum Hall effect [15]. One of the most surprising characteristics of BP is its strong response to external electric and strain fields. As a consequence, the electronic and optical properties of this material can be efficiently tuned by applying an external bias voltage [16–20] or by strain engineering [21–25]. In particular, it is possible to drive a semiconductor-to-semimetal transition, with the appearance of a Dirac-like dispersion [16–18,26].

In this paper we study the electronic spectrum of biased BP in the presence of a strong magnetic field. For this we use a tight-binding model which properly accounts for the band structure in a wide energy window of the spectrum [27,28]. The electronic density of states (DOS) is calculated from the solution of the time-dependent Schrödinger equation within the framework of the tight-binding propagation method [29–31], which is an efficient numerical tool in large-scale calculations of realistic systems with more than millions of atoms. In the absence, or for moderate values, of the applied bias, the obtained Landau level (LL) quantization is that of a standard two-dimensional electron gas (2DEG) with a set of equidistant LLs [32–34]. When the applied electric field is strong enough, the BP suffers a semiconductor-to-semimetal transition, with the appearance of a set of nonequidistant LLs, associated with Dirac-like cones that emerge in the spectrum. Such an LL spectrum resembles that of graphene in the quantum Hall regime, with the difference that

biased BP presents a pronounced electron-hole asymmetry. As we increase the energy, the spectrum acquires a highly nontrivial quantization due to the presence of a Van Hove singularity, with a corresponding change in the topological Berry phase. We further calculated the Hall conductivity from the Kubo-Bastin formula [35], in the context of the kernel polynomial method [36,37]. We find that unbiased BP presents the characteristic integer quantum Hall effect with $\sigma_{xy}^{\text{IQHE}} = 2n(e^2/h)$, whereas biased semimetal BP presents a *relativistic* quantum Hall effect characteristic of Dirac materials, with $\sigma_{xy}^{\text{RQHE}} = 4(n + 1/2)(e^2/h)$ [38]. Although we perform the numerical calculations for the simplest case of bilayer BP, the physical results should hold for any multilayer sample exposed to external magnetic and electric fields.

II. ELECTRONIC BAND STRUCTURE AND LANDAU QUANTIZATION

BP is formed by stacking of phosphorene layers, coupled with a van der Waals interaction. Single-layer BP contains two atomic layers and two kinds of P-P bonds (in-plane and interplane) [4], as shown in Fig. 1. Our calculations are done using a GW -based tight-binding model that properly reproduces the conduction and valence bands in an energy range ~ 0.3 eV beyond the gap [27,28],

$$\mathcal{H} = \sum_{i \neq j} t_{ij} c_i^\dagger c_j + \sum_{i \neq j} t_{p,ij} c_i^\dagger c_j, \quad (1)$$

where c_i^\dagger (c_i) creates (annihilates) an electron at site i , and 10 intralayer t_{ij} and 5 interlayer $t_{p,ij}$ hopping terms are considered in the model. The values of the 10 intralayer hopping terms [shown in Fig. 1(a)] are $t_1 = -1.486$ eV, $t_2 = 3.729$ eV, $t_3 = -0.252$ eV, $t_4 = -0.071$ eV, $t_5 = -0.019$ eV, $t_6 = -0.186$ eV, $t_7 = -0.063$ eV, $t_8 = 0.101$ eV, $t_9 = -0.042$ eV, $t_{10} = -0.073$ eV, and the 5 interlayer hopping terms [Fig. 1(b)] are $t_{p1} = 0.524$ eV, $t_{p2} = 0.180$ eV, $t_{p3} = -0.123$ eV, $t_{p4} = -0.168$ eV, $t_{p5} = 0.005$ eV [28]. The effect of an electric field on the electronic dispersion is considered by introducing linearly a biased on-site potential difference

*s.yuan@science.ru.nl

†rroldan@icmm.csic.es

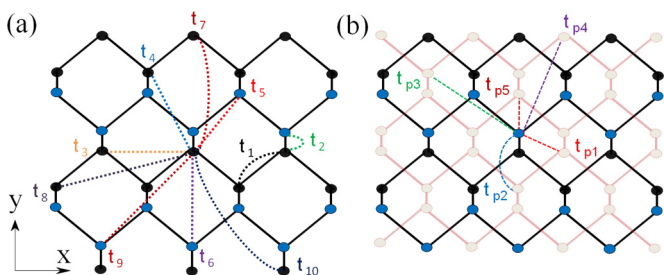


FIG. 1. Lattice structure of single-layer (a) and bilayer (b) black phosphorus. Circles of different colors correspond to atoms located in different planes within a single puckered layer. The relevant hopping terms considered in Hamiltonian (1) are indicated: 10 in-plane hopping terms (a) and 5 interlayer terms (b).

between the outmost planes of two layers, without considering the screening effect. For example, in a single layer we include a different on-site potential $\pm\Delta/2$ in the top and bottom sublayers, respectively, whereas in a bilayer BP we include a sequence of on-site potentials in the four planes with the form $\Delta/2 + v_b\Delta$, $\Delta/2 - v_b\Delta$, $-\Delta/2 + v_b\Delta$, and $-\Delta/2 - v_b\Delta$, where $v_b = 0.202$ is a linear scaling factor accounting for the lattice position along the direction of the external electric field [28]. Figure 2 shows the band structure obtained from the tight-binding model, (1), for three representative cases, and their corresponding constant-energy contours (CECs) are shown in Fig. 3. As is well known [4] for unbiased BP ($\Delta = 0$) the band structure corresponds to an anisotropic direct band-gap semiconductor, with the gap placed at the Γ point of the Brillouin zone.

It is interesting to consider the different effects of a perpendicular electric field in the band structure of single-layer versus multilayer BP. In Fig. 4 we show the evolution of the band gap at the Γ point as a function of the biased potential, defined from the energy difference between the valence and the conduction band edges as obtained from the full tight-binding model, (1). We observe that, whereas the gap increases with Δ in single-layer BP, the gap in bilayer BP decreases with the applied bias, and eventually a semiconductor-to-semimetal transition takes place. A similar closing of the gap with the bias potential occurs for any multilayer sample. The opposite behavior between single-layer and multilayer BP can be

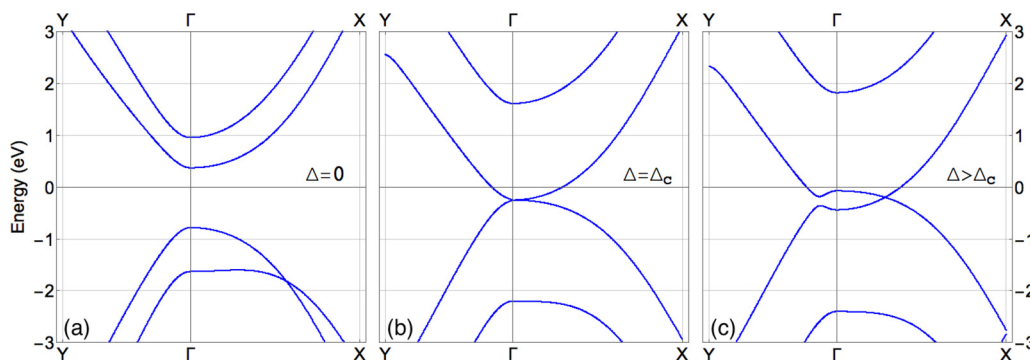


FIG. 2. Band structure of biased bilayer BP for three representative values of the applied voltage: unbiased ($\Delta = 0$), for which the system is gapped; $\Delta = \Delta_c$, for which the gap closes and there is a band crossing at the Γ point; and $\Delta > \Delta_c$, corresponding to the semimetal phase with the creation of Dirac points in the Γ -X direction of the Brillouin zone.

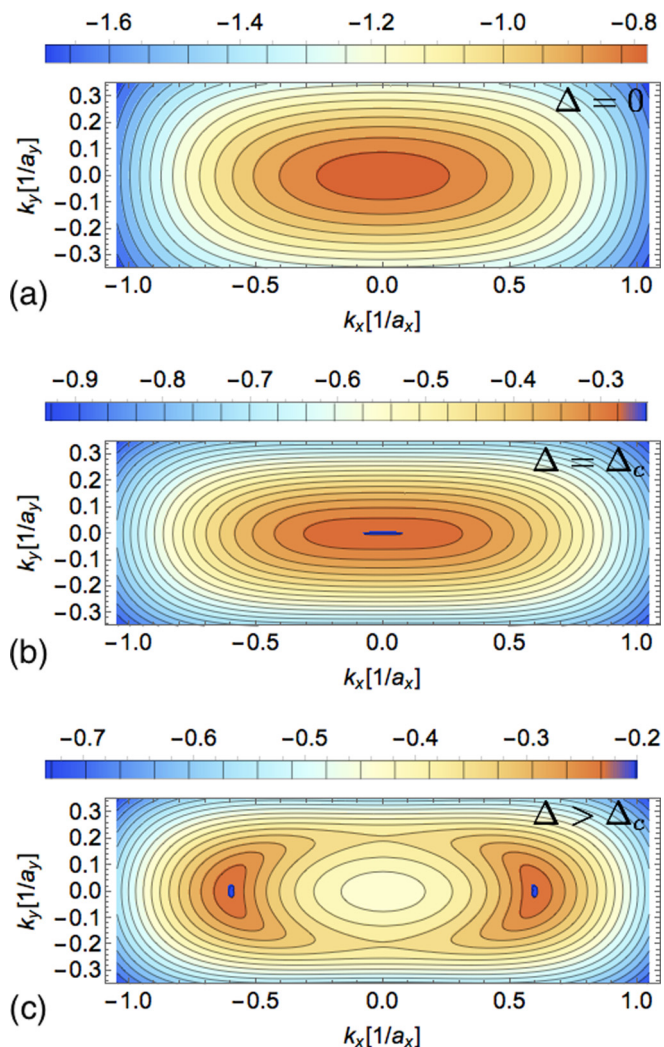


FIG. 3. Constant energy contours of biased bilayer BP for the three values of the applied voltage used in Fig. 2. For $\Delta > \Delta_c$, corresponding to the semimetal phase with the creation of Dirac points in the Γ -X direction of the Brillouin zone.

understood analytically by using the tight-binding model, (1), with only the leading hopping terms, namely, t_1 , t_2 , and t_{p1} . In the absence of a perpendicular electric field, $\Delta = 0$, the gap

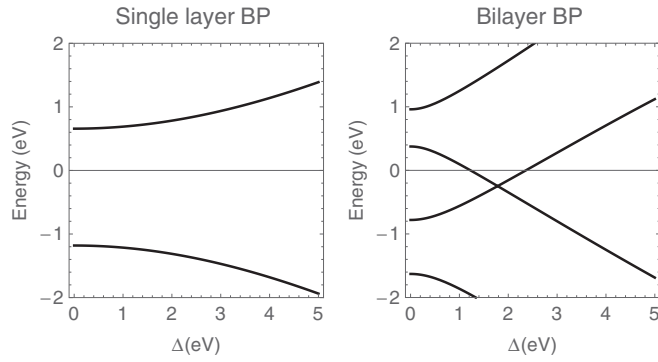


FIG. 4. Evolution of the valence and conduction band edges at the Γ point as a function of the biased potential Δ , for single-layer and bilayer BP, as calculated from the full tight-binding model, (1). The dashed line in (b) indicates the chemical potential energy in the semimetal phase.

in single-layer BP is controlled by the difference between the in-plane hopping parameter t_1 and the interplane t_2 ,

$$E_{g1L}(\Delta = 0) \approx 4t_1 + 2t_2, \quad (2)$$

where it is important to note the different signs of the two terms, $t_1 \approx -1.5$ eV < 0 and $t_2 \approx 3.7$ eV > 0 . For bilayer BP, the gap at $\Delta = 0$ is approximately given by

$$E_{g2L}(\Delta = 0) \approx 4t_1 + 2\sqrt{t_2^2 + 2t_{p1}^2} - 2|t_{p1}|\sqrt{t_2^2 + t_{p1}^2}. \quad (3)$$

Note that the interlayer hopping t_{p1} in bilayer BP enters into the gap equation as an extra contribution to the interplane hopping term in single-layer BP, t_2 . In the presence of a biased potential, and within the above approximation, the gap in single-layer BP can be expressed as

$$E_{g1L} \approx 4t_1 + 2\sqrt{t_2^2 + \left(\frac{\Delta}{2}\right)^2}, \quad (4)$$

whereas for bilayer BP the gap is given by

$$E_{g2L} \approx 4t_1 + 2\sqrt{t_2^2 + \left(\frac{\Delta}{2}\right)^2} + f_{\text{inter}}, \quad (5)$$

where we have defined

$$f_{\text{inter}} = 2t_{p1}^2 + v_b^2 \Delta^2 - \sqrt{t_2^2(4t_{p1}^2 + \Delta^2) + (-2t_{p1}^2 + v_b \Delta^2)^2}. \quad (6)$$

One can easily see that, for the hopping parameters of the model, there is no real solution for Δ that closes the gap in single-layer BP, which should fulfill $\Delta_{1L}^c \approx 2\sqrt{4t_1^2 - t_2^2}$. Therefore, this simple analytical analysis shows that application of a perpendicular electric field has the effect of opening the gap in single-layer BP, in agreement with the full tight-binding results shown in Fig. 4. Bilayer BP, on the other hand, has a real solution for the closing of the gap. The analytical expression is too long to be given here, but one can simply observe that the term f_{inter} , as defined in Eq. (6), is < 0 . This leads to a correction for the second contribution in the gap equation, (5), which can fully cancel

the $4t_1$ term, driving a semiconductor-to-semimetal transition. From now on, we focus on the multilayer case, for which the aforementioned transition can take place in the presence of a bias potential. The topological nature of the transition has been addressed by Liu *et al.* [17] by combining DFT and group theory analysis [17]. Semiconducting unbiased BP has valence and conduction bands with different symmetric representations at the Γ point (point group D_{2h}): the conduction band has the representation $A_g(\Gamma_1)$, whereas the valence band has the representation $B_{3u}(\Gamma_8)$. One can define the inversion energy as $\Delta_{\text{inv}} = E_{\Gamma_1} - E_{\Gamma_8}$. When the bias voltage is high enough, the gap is 0 and Δ_{inv} becomes negative, indicating a band inversion. This band inversion is accompanied by a Dirac-like band crossing, as shown in Fig. 2. This band crossing is protected by fractional translation symmetry due to the different characters of the two bands. Therefore, the spectrum can be described at low energies by a 2×2 Dirac equation. The analysis of the wave function performed in Ref. [17] for multilayer samples reveals that the Γ_1 states are mainly localized in the top layer, whereas the spectral weight of the Γ_8 states is stronger in the bottom layer.

We insist that the approximation considered here does not take into account electrostatic screening due to the external electric field. This effect has been studied in Ref. [9], using a low-energy continuum model and within nonlinear Thomas-Fermi theory. The potential difference across a BP sample obtained there suggests that BP presents an intermediate screening behavior between the strong-coupling limit of graphene, where the carriers concentrate close to the interface, and the weak-coupling regime with reduced screening properties that dominates the screening of other van der Waals semiconducting materials such as MoS₂.

The presence of a magnetic field is accounted for by means of the Peierls substitution, which replaces the hopping term between two sites,

$$t_{ij} \rightarrow t_{ij} \exp \left[i \frac{2\pi}{\Phi_0} e \int_{\mathbf{R}_i}^{\mathbf{R}_j} \mathbf{A} \cdot d\mathbf{l} \right], \quad (7)$$

where $\Phi_0 = hc/e$ is the flux quantum and $\mathbf{A} = (-By, 0, 0)$ is the vector potential in the Landau gauge, B being the strength of the magnetic field. The band structure can now be calculated by choosing a ribbon with 1 unit cell width and a height that exactly matches the period of the Peierls phase. After obtaining the Hamiltonian as a function of the momentum,

$$\mathcal{H}(\mathbf{k}) = \sum_{i \neq j} t_{ij} c_i^\dagger c_j e^{i\mathbf{k} \cdot (\mathbf{r}_i - \mathbf{r}_j)} + \sum_{i \neq j} t_{p,ij} c_i^\dagger c_j e^{i\mathbf{k} \cdot (\mathbf{r}_i - \mathbf{r}_j)}, \quad (8)$$

the energy eigenvalues corresponding to a momentum \mathbf{k} can be found with exact diagonalization. Our results lead to a band structure composed of a set of LLs, as given in Fig. 5. The structure of the LL spectrum is discussed in detail later.

The DOS of the system is calculated by using an algorithm based on the evolution of the time-dependent Schrödinger equation. For this we use a random superposition of all basis states as the initial state $|\varphi\rangle$

$$|\varphi\rangle = \sum_i a_i |i\rangle, \quad (9)$$

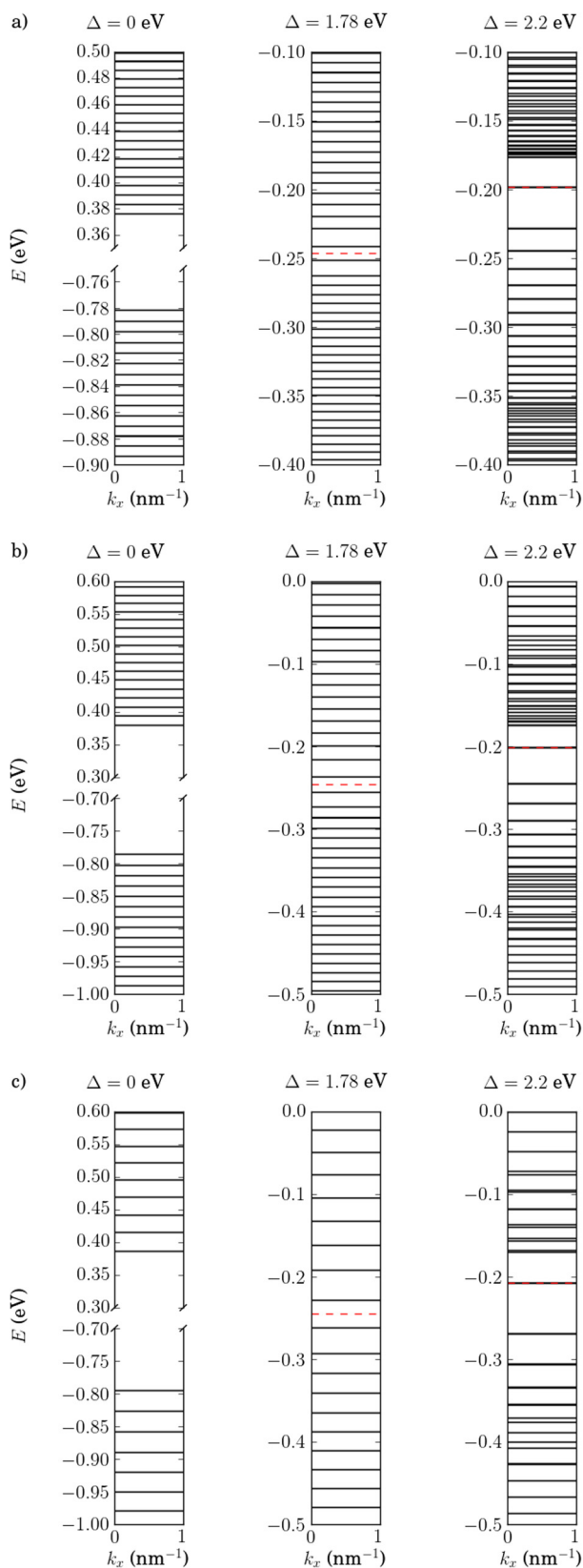


FIG. 5. Landau level structure obtained from exact diagonalization of Hamiltonian (8) for (a) $B = 32.5$ T, (b) $B = 65$ T, and (c) $B = 130$ T. The Fermi level is indicated by the dashed red line and falls in the gap (skipped regions) for $\Delta = 0$.

where a_i are random complex numbers normalized as $\sum_i |a_i|^2 = 1$, and the DOS is calculated as a Fourier transform of the time-dependent correlation functions [29,39],

$$d(\epsilon) = \frac{1}{2\pi} \int_{-\infty}^{\infty} e^{i\epsilon\tau} \langle \varphi | e^{-iH\tau} | \varphi \rangle d\tau. \quad (10)$$

In the unbiased semiconducting phase ($\Delta = 0$) the DOS (per unit area) at low energies is approximately a constant $d_{2\text{DEG}}(\epsilon) = gm_b/2\pi$ where $g = g_s = 2$ is the spin degeneracy and $m_b^{c,v} = \sqrt{m_x^{c,v} m_y^{c,v}}$ is the band mass of the conduction (c) or valence (v) bands, as obtained in Fig. 6(a). In the presence of a quantifying magnetic field, the DOS is discretized into a set of Landau levels, as shown in Fig. 6(d) (see also Fig. 5). We note that the finite broadening in the LLs is due to the energy resolution of the numerical simulations, which is limited by the size of the sample used in the calculation (number of atoms), as well as the total number of time steps, which determines the accuracy of the energy eigenvalues. The obtained LL spectrum consist of two sets of equidistant LLs separated by the band gap E_g with energy $\epsilon_n^{c,v} = \pm E_g/2 \pm \omega_c^{c,v}(n + 1/2)$ (where n is a positive integer) separated by the cyclotron frequency $\omega_c^{c,v} = eB/m_b^{c,v}$. Since the system lacks electron-hole symmetry, the cyclotron frequency is different for the valence and conduction bands. For $\Delta = \Delta_c = 1.783$ eV, the system suffers a semiconducting-to-semimetal transition, with a band crossing at the Γ point [see Fig. 2(b)]. As shown in Fig. 6(b), the DOS around such a band crossing is $\propto \sqrt{\epsilon}$, leading to a set of nonequidistant LLs at energies close to the band crossing energy, with dispersion $\epsilon_n \propto \pm[(n + 1/2)B]^{2/3}$ [40,41]. As we move away from this band crossing, the LL spectrum has the same characteristics as in the previous case of unbiased BP, recovering the standard quantization of a 2DEG [Fig. 6(e)].

The most interesting situation occurs for higher bias voltages, well beyond the transition. For $\Delta = 2.2$ eV $> \Delta_c$, the band dispersion presents two Dirac points, in the Γ - X direction, and it is gapped in the Γ - Y direction [see Figs. 2(c) and 3(c)]. As studied by Montambaux *et al.* within the framework of a universal Hamiltonian that describes the merging of Dirac points in the electronic spectrum of two-dimensional crystals [41,42], the topological character of the transition can be understood from the appearance of a Berry phase for $\Delta > \Delta_c$, which takes the values $\pm\pi$ around each Dirac point. If we reduce the bias voltage, we recover the trivial phase with the corresponding annihilation of the Berry phase for $\Delta < \Delta_c$. For low carrier densities, the Fermi surface consists of two pockets encircling the Dirac points along the Γ - X direction [see Fig. 3(c)]. The DOS close to the Dirac points behaves as [41] $d_{\text{Dirac}}(\epsilon) \propto |\epsilon|/v_{F_x}v_{F_y}$, where $v_{F_x(y)}$ is the Fermi velocity along the $x(y)$ direction within the Dirac cones. In a magnetic field, the LL spectrum is that of a semimetal with a *relativistic* quantization, $\epsilon_n \propto \pm\sqrt{nB}$ [see Fig. 6(f)]. The shift of $n + 1/2 \rightarrow n$ in the LL energy spectrum for $\Delta > \Delta_c$ is a consequence of the generation of $\pm\pi$ Berry phases around the Dirac points. If we increase the energy, we reach a highly nontrivial LL quantization because of the presence of a saddle point in the band structure, at which there is a transition from CECs encircling the Dirac points to CECs encircling the Γ point. In the semiclassical limit, the cyclotron

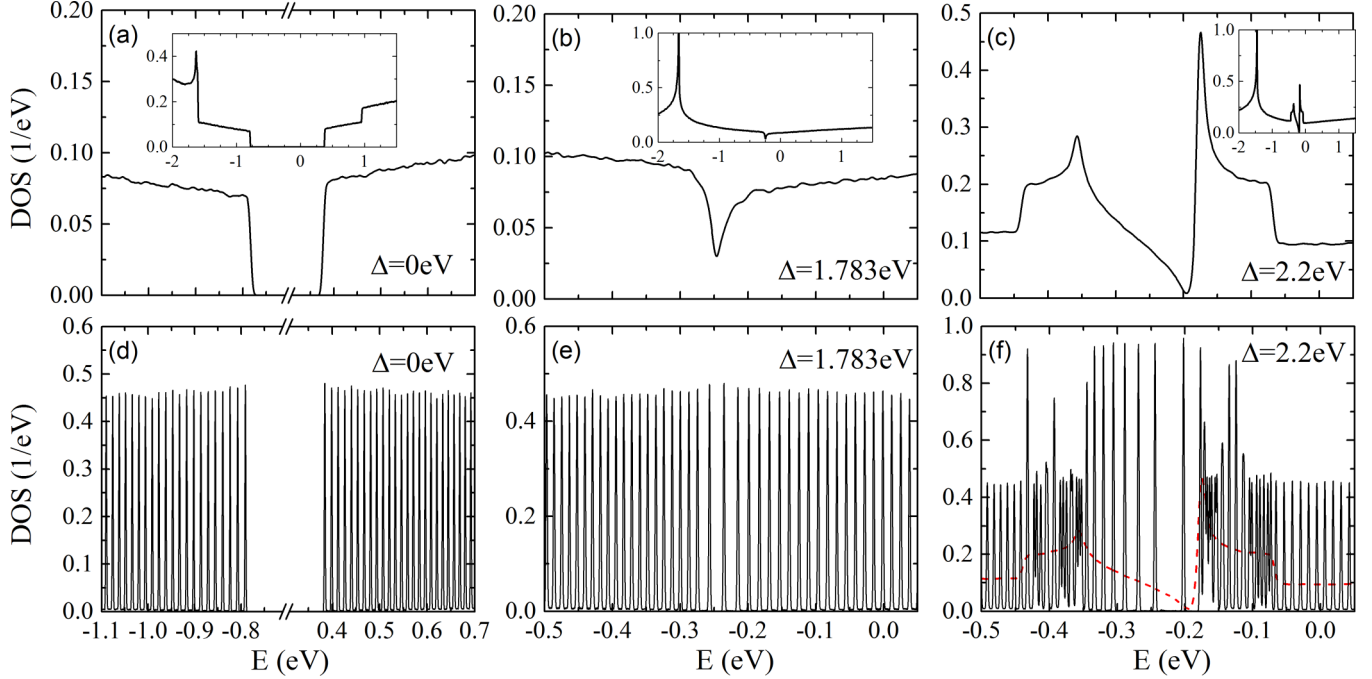


FIG. 6. Density of states and Landau level spectra of pristine and biased bilayer BP for the biased potential indicated. (a–c) $B = 0$ and (d–f) $B = 65$ T. The calculated system contains $2 \times 4800 \times 4800$ atomic sites, with periodic boundary conditions in both the X and the Y directions. To illustrate the evolution with a magnetic field of the DOS of the semimetallic phase ($\Delta = 2.2$ eV), we include in (f) the DOS at $B = 0$ (dashed red line).

orbits in reciprocal space follow the CECs. Therefore, at the saddle point there is a change in the topological Berry phase from $\pm\pi$ for orbits encircling the Dirac points to 0 for orbits encircling the Γ point [43,44]. The two series of LLs shown in Fig. 6 is due to the different characters of the cyclotron orbits at both sides of the saddle point, with different cyclotron frequencies, that *merge* at the saddle point. This transition resembles that of highly doped graphene at energies around the Van Hove singularity [45,46].

III. HALL CONDUCTIVITY

The next step in our analysis, once we understand the LL spectrum of the biased system, is the calculation of the Hall conductivity σ_{xy} . For this aim, we use an efficient numerical approach, recently developed by García *et al.* [36], that is based on a real-space implementation of the Kubo formalism where both diagonal and off-diagonal conductivities are treated on the same footing. In the limit $\omega \rightarrow 0$ and for noninteracting electrons, the so-called Kubo-Bastin formula for the conductivity can be used to obtain the elements of the static conductivity tensor [35–37],

$$\sigma_{\alpha\beta}(\mu, T) = \frac{i\hbar e^2}{A} \int_{-\infty}^{\infty} d\varepsilon f(\varepsilon) \text{Tr} \left\langle v_{\alpha} \delta(\varepsilon - \mathcal{H}) v_{\beta} \frac{dG^{+}(\varepsilon)}{d\varepsilon} - v_{\alpha} \frac{dG^{-}(\varepsilon)}{d\varepsilon} v_{\beta} \delta(\varepsilon - \mathcal{H}) \right\rangle, \quad (11)$$

where μ is the chemical potential, T is the temperature, A is the area of the sample, v_{α} is the α component of the velocity operator, $G^{\pm}(\varepsilon) = 1/(\varepsilon - \mathcal{H} \pm i\eta)$ are the Green's functions, and $f(\varepsilon)$ is the Fermi-Dirac distribution. Here the average is

performed by using the same random initial state as in the calculation of DOS. By expanding the delta and the Green's functions $G^{\pm}(\varepsilon)$ in terms of Chebyshev polynomials (using the so-called kernel polynomial method) [36], the conductivity tensor becomes

$$\sigma_{\alpha\beta}(\mu, T) = \frac{4e^2\hbar}{\pi A} \frac{4}{\Delta E^2} \int_{-1}^1 d\tilde{\varepsilon} \frac{f(\tilde{\varepsilon})}{(1 - \tilde{\varepsilon}^2)^2} \sum_{m,n} \Gamma_{nm}(\tilde{\varepsilon}) \mu_{nm}^{\alpha\beta}(\tilde{H}), \quad (12)$$

where ΔE is the energy range of the spectrum, $\tilde{\varepsilon}$ is the rescaled energy within $[-1, 1]$, $\Gamma_{mn}(\tilde{\varepsilon})$ and $\mu_{mn}^{\alpha\beta}(\tilde{H})$ are functions of the energy and the Hamiltonian, respectively. More precisely,

$$\Gamma_{mn}(\tilde{\varepsilon}) \equiv T_m(\tilde{\varepsilon})(\tilde{\varepsilon} - in\sqrt{1 - \tilde{\varepsilon}^2})e^{in \arccos(\tilde{\varepsilon})} + T_n(\tilde{\varepsilon})(\tilde{\varepsilon} + im\sqrt{1 - \tilde{\varepsilon}^2})e^{-im \arccos(\tilde{\varepsilon})} \quad (13)$$

is a scalar function of the rescaled energy, and

$$\mu_{mn}^{\alpha\beta}(\tilde{H}) \equiv \frac{g_m g_n}{(1 + \delta_{n0})(1 + \delta_{m0})} \text{Tr}[v_{\alpha} T_m(\tilde{H}) v_{\beta} T_n(\tilde{H})] \quad (14)$$

is independent of the energy, where $T_m(x)$ is the Chebyshev polynomial defined according to the recurrence relation $T_m(x) = 2xT_{m-1}(x) - T_{m-2}(x)$ with $T_0(x) = 1$ and $T_1(x) = x$. The Gibbs oscillations due to the truncation of the expansion in (12) are smoothed by using the Jackson kernel g_m [36,47].

Our results for σ_{xy} are shown in Fig. 7. For $\Delta = 0$ the Hall conductivity consists of a series of plateaus with the well-known sequence $\sigma_{xy} = 2ne^2/h$, characteristics of a standard 2DEG with a parabolic band dispersion (although the present case of BP is rather described by a paraboloidal band). Our numerical calculations show the same quantization of the

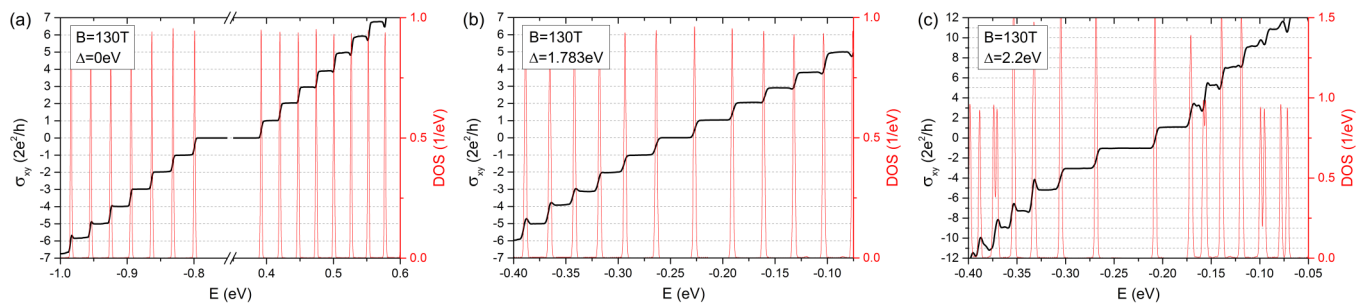


FIG. 7. Hall conductivity of pristine and biased BP for the biased potentials used in Fig. 6. The temperature is $T = 0.01$ K and the magnetic field is $B = 130$ T. The truncation order for the kernel polynomial in Eq. (12) is $M = 15\,000$. The calculated system contains $2 \times 600 \times 600$ atomic sites, and the results are averaged over five random realizations of initial states.

Hall conductivity at the transition point $\Delta = \Delta_c$ [Fig. 7(c)]. This is due to the fact that, right at the transition, there is a single crossing of the bands at the time-reversal-invariant Γ point of the Brillouin zone [41,42]. Most saliently, for $\Delta > \Delta_c$ [Fig. 7(c)] the Hall conductivity presents plateaus at $\sigma_{xy} = 4(n + 1/2)e^2/h$. This is due to the topological nature of the semimetallic phase, which is well captured by the numerical method. The plateau structure becomes blurred at high energies, which is an artifact due to the finite truncation order of the kernel polynomial approximation as well as the finite size of the sample [36]. These artifacts can be improved with a higher truncation order of the expansion and by considering a larger sample size. This would lead to an initial state, obtained from Eq. (9), that is a more accurate representation of the whole energy spectrum [29,39]. Furthermore, it has been shown that the convergence of the Hall conductivity in Eq. (12) is faster with larger magnetic fields [36]. Therefore, in order to catch several Landau levels within the emerged Dirac cones, the large magnetic field of $B = 130$ T is used in the calculations. Lower magnetic fields will give similar qualitative behaviors for the LL spectrum and for the Hall conductivity. In spite of the above choices in the simulation, the convergence of the results is still slow, especially if the band structure contains different topological features within a small energy range, such as in the case with $\Delta > \Delta_c$. We adopted a truncation order as large as $M = 15\,000$ for the kernel polynomial decomposition (the computational costs are proportional to M^2 and the maximum truncation order used in Ref. [36] is $M = 6144$), and the simulated systems consist of $2 \times 600 \times 600$ atomic sites. However, it is still not enough to overcome the blurred effects in the high-energy plateaus. Further calculations with a larger truncation order or sample size are beyond the computational resource that we can reach.

IV. DISCUSSION AND CONCLUSIONS

We note that the emergence of Dirac points in the spectrum of biased black phosphorus can be understood by thinking of the BP lattice as a honeycomb lattice (like the one in graphene) in which one of the three hopping terms between nearest-neighbor atoms can be different from the other two [41]. This is indeed the case in BP, in which two of the three nearest neighbors of one atom are on the same plane, whereas the third nearest neighbor is on a different plane. Moreover, the

signs of these hopping terms are different, making BP a natural platform to realize Dirac point engineering near the Γ point [42], either by tuning the external bias or by applying strain to the samples.

In summary, we have analyzed the electronic properties of biased black phosphorus in the presence of a perpendicular magnetic field. In the absence of an electric field, the external magnetic field leads to a quantization of the electron and hole bands into a set of equidistant Landau levels. This behavior is similar to the discretization of the energy dispersion in a 2DEG with a parabolic band. If we further apply a perpendicular electric field to the sample, we obtain a reduction of the band gap with the applied voltage. For a critical value of the voltage, the gap completely closes, and a pair of Dirac points appears in the Γ -X direction of the Brillouin zone. This semiconductor-to-semimetal transition is accompanied by a change in the topology of the system, due to the generation of $\pm\pi$ Berry phases around the Dirac points. We obtain a highly nontrivial LL spectrum in this phase, with the coexistence of relativistic LLs, with a $\varepsilon_n \propto \sqrt{nB}$ quantization, with equidistant LLs at higher energies, following the standard $\varepsilon_n \propto B(n + 1/2)$, characteristic of a 2DEG. The transition between these two regimes requires going through a Van Hove singularity (saddle point) in the band dispersion, with the corresponding divergence in the DOS. Finally, we numerically compute the Hall conductivity of the system. The topological transition driven by the electric field is reflected in a different quantization of the Hall conductivity, which presents the characteristic $\sigma_{xy} \propto 2n$ behavior for low bias voltages (insufficient to close the gap) and a *relativistic* quantum Hall effect with $\sigma_{xy} \propto 4(n + 1/2)$ in the semimetallic phase, due to the generation of a pair of Dirac cones. Although we focus on the simplest case of bilayer BP, the results presented here apply to any multilayer BP sample, with the advantage that the gap decreases with the number of layers, and therefore the semiconducting-to-semimetal transition would be more easily reached for thicker samples. We note that the electric-field-induced semimetallic phase in BP is likely to present new broken-symmetry phases due to many-body effects, which are not included here. For example, it is known that bilayer graphene, whose low-energy spectrum reassembles that of biased semimetallic BP, suffers a nematic phase transition driven by Coulomb interactions [48]. Similar interaction-driven phase transitions might occur in BP and will be the object of future studies. The phenomena discussed

here could be observed by exposing a biased BP sample, chemically doped from *in situ* deposition of adatoms [16], to a strong quantizing magnetic field or by applying external strain (compression) to the samples [23]. These techniques have been shown to be appropriate routes to tune this material from a moderate-gap semiconductor to a band-inverted semimetal.

ACKNOWLEDGMENTS

We are grateful to G. Montambaux, J.-N. Fuchs, and M. O. Goerbig for very useful discussions. The support

from the Stichting Fundamenteel Onderzoek der Materie (FOM) and The Netherlands National Computing Facilities foundation (NCF) is acknowledged. S.Y. and M.I.K. acknowledge financial support from the European Research Council Advanced Grant program (Contract No. 338957). This project received funding from the European Unions Horizon 2020 research and innovation program under Grant Agreement No. 696656 GrapheneCore1. R.R. acknowledges financial support from MINECO (Spain) through Grant No. FIS2014-58445-JIN and from the Comunidad Autónoma de Madrid (CAM) MAD2D-CM Program (S2013/MIT-3007) under Project No. PIB2010BZ-00512.

-
- [1] L. Li, Y. Yu, G. J. Ye, Q. Ge, X. Ou, H. Wu, D. Feng, X. H. Chen, and Y. Zhang, *Nat. Nanotechnol.* **9**, 372 (2014).
- [2] F. Xia, H. Wang, and Y. Jia, *Nat. Commun.* **5**, 4458 (2014).
- [3] A. Castellanos-Gomez, *J. Phys. Chem. Lett.* **6**, 4280 (2015).
- [4] A. Morita, *Appl. Phys. A* **39**, 227 (1986).
- [5] H. Liu, A. T. Neal, Z. Zhu, Z. Luo, X. Xu, D. Tománek, and P. D. Ye, *ACS Nano* **8**, 4033 (2014).
- [6] J. Qiao, X. Kong, Z.-X. Hu, F. Yang, and W. Ji, *Nat. Commun.* **5**, 4475 (2014).
- [7] T. Low, A. S. Rodin, A. Carvalho, Y. Jiang, H. Wang, F. Xia, and A. H. Castro Neto, *Phys. Rev. B* **90**, 075434 (2014).
- [8] S. Yuan, A. N. Rudenko, and M. I. Katsnelson, *Phys. Rev. B* **91**, 115436 (2015).
- [9] T. Low, R. Roldán, H. Wang, F. Xia, P. Avouris, L. M. Moreno, and F. Guinea, *Phys. Rev. Lett.* **113**, 106802 (2014).
- [10] X. Chen, Y. Wu, Z. Wu, S. Xu, L. Wang, Y. Han, W. Ye, T. Han, Y. He, Y. Cai *et al.*, *Nat. Commun.* **6**, 7315 (2014).
- [11] N. Gillgren, D. Wickramaratne, Y. Shi, T. Espiritu, J. Yang, J. Hu, J. Wei, X. Liu, Z. Mao, K. Watanabe *et al.*, *2D Mater.* **2**, 011001 (2015).
- [12] L. Li, G. J. Ye, V. Tran, R. Fei, G. Chen, H. Wang, J. Wang, K. Watanabe, T. Taniguchi, L. Yang *et al.*, *Nat. Nanotechnol.* **10**, 608 (2015).
- [13] V. Tayari, N. Hemsworth, I. Fasih, A. Favron, E. Gaufrès, G. Gervais, R. Martel, and T. Szkopek, *Nat. Commun.* **6**, 7702 (2014).
- [14] Y. Cao, A. Mishchenko, G. Yu, K. Khestanova, A. Rooney, E. Prestat, A. Kretinin, P. Blake, M. Shalom, G. Balakrishnan *et al.*, *Nano Lett.* **15**, 4914 (2015).
- [15] L. Li *et al.*, *Nature Nanotechnology*, doi: 10.1038/nnano.2016.42.
- [16] J. Kim, S. S. Baik, S. H. Ryu, Y. Sohn, S. Park, B.-G. Park, J. Denlinger, Y. Yi, H. J. Choi, and K. S. Kim, *Science* **349**, 723 (2015).
- [17] Q. Liu, X. Zhang, L. B. Abdalla, A. Fazzio, and A. Zunger, *Nano Lett.* **15**, 1222 (2015).
- [18] K. Dolui and S. Y. Quek, *Sci. Rep.* **5**, 11699 (2015).
- [19] A. Chaves, T. Low, P. Avouris, D. Çakır, and F. M. Peeters, *Phys. Rev. B* **91**, 155311 (2015).
- [20] S. S. Baik, K. S. Kim, Y. Yi, and H. J. Choi, *Nano Lett.* **15**, 7788 (2015).
- [21] A. S. Rodin, A. Carvalho, and A. H. Castro Neto, *Phys. Rev. Lett.* **112**, 176801 (2014).
- [22] R. Roldán, A. Castellanos-Gomez, E. Cappelluti, and F. Guinea, *J. Phys. Condens. Matter* **27**, 313201 (2015).
- [23] Z. J. Xiang, G. J. Ye, C. Shang, B. Lei, N. Z. Wang, K. S. Yang, D. Y. Liu, F. B. Meng, X. G. Luo, L. J. Zou *et al.*, *Phys. Rev. Lett.* **115**, 186403 (2015).
- [24] J. Quereda, P. San-Jose, V. Parente, L. Vaquero-Garzon, A. J. Molina-Mendoza, N. Agrat, G. Rubio-Bollinger, F. Guinea, R. Roldán, and A. Castellanos-Gomez, *Nano Lett.* **16**, 2931 (2016).
- [25] A. Manjanath, A. Samanta, T. Pandey, and A. K. Singh, *Nanotechnol.* **26**, 075701 (2015).
- [26] F. Jin, R. Roldán, M. I. Katsnelson, and S. Yuan, *Phys. Rev. B* **92**, 115440 (2015).
- [27] A. N. Rudenko and M. I. Katsnelson, *Phys. Rev. B* **89**, 201408 (2014).
- [28] A. N. Rudenko, S. Yuan, and M. I. Katsnelson, *Phys. Rev. B* **92**, 085419 (2015).
- [29] S. Yuan, H. De Raedt, and M. I. Katsnelson, *Phys. Rev. B* **82**, 115448 (2010).
- [30] S. Yuan, R. Roldán, and M. I. Katsnelson, *Phys. Rev. B* **84**, 035439 (2011).
- [31] S. Yuan, T. O. Wehling, A. I. Lichtenstein, and M. I. Katsnelson, *Phys. Rev. Lett.* **109**, 156601 (2012).
- [32] J. M. Pereira and M. I. Katsnelson, *Phys. Rev. B* **92**, 075437 (2015).
- [33] Y. Jiang, R. Roldán, F. Guinea, and T. Low, *Phys. Rev. B* **92**, 085408 (2015).
- [34] X. Zhou, R. Zhang, J. Sun, Y. Zou, G. Zhou, F. Zhai, and K. Chang, *Sci. Rep.* **5**, 12295 (2015).
- [35] A. Bastin, C. Lewiner, O. Betbeder-Matibet, and P. Nozieres, *J. Phys. Chem. Solids* **32**, 1811 (1971).
- [36] J. H. García, L. Covaci, and T. G. Rappoport, *Phys. Rev. Lett.* **114**, 116602 (2015).
- [37] F. Ortmann, N. Leconte, and S. Roche, *Phys. Rev. B* **91**, 165117 (2015).
- [38] M. Goerbig, *Rev. Mod. Phys.* **83**, 1193 (2011).
- [39] A. Hams and H. De Raedt, *Phys. Rev. E* **62**, 4365 (2000).
- [40] P. Dietl, F. Piéchon, and G. Montambaux, *Phys. Rev. Lett.* **100**, 236405 (2008).
- [41] G. Montambaux, F. Piéchon, J.-N. Fuchs, and M. O. Goerbig, *Eur. Phys. J. B* **72**, 509 (2009).
- [42] G. Montambaux, F. Piéchon, J.-N. Fuchs, and M. O. Goerbig, *Phys. Rev. B* **80**, 153412 (2009).
- [43] J. Fuchs, F. Piéchon, M. Goerbig, and G. Montambaux, *Eur. Phys. J. B* **77**, 351 (2010).

- [44] R. de Gail, M. O. Goerbig, and G. Montambaux, *Phys. Rev. B* **86**, 045407 (2012).
- [45] Y. Hatsugai, T. Fukui, and H. Aoki, *Phys. Rev. B* **74**, 205414 (2006).
- [46] S. Yuan, R. Roldán, and M. I. Katsnelson, *Solid State Commun.* **152**, 1446 (2012).
- [47] A. Weiße, G. Wellein, A. Alvermann, and H. Fehske, *Rev. Mod. Phys.* **78**, 275 (2006).
- [48] A. Mayorov, D. Elias, M. Mucha-Kruczynski, R. Gorbachev, T. Tudorovskiy, A. Zhukov, S. Morozov, M. Katsnelson, V. Fal'ko, A. Geim *et al.*, *Science* **333**, 860 (2011).